ISSN 1674-1056
http://cpb.iphy.ac.cn
http://iopscience.iop.org/cpb
中国物理 B
Chinese Physics
中国物理
Chinese Physics B

Broadband microwave absorption properties of polyurethane foam absorber optimized by sandwiched cross-shaped metamaterial

Long-Hui He(贺龙辉), Lian-Wen Deng(邓联文), Heng Luo(罗衡), Jun He(贺君), Yu-Han Li(李宇涵), Yun-Chao Xu(徐运超), Sheng-Xiang Huang(黄生祥)

Citation: Chin. Phys. B . 2018, 27(12): 127801. **doi:** 10.1088/1674-1056/27/12/127801
Journal homepage: http://cpb.iphy.ac.cn; http://iopscience.iop.org/cpb

What follows is a list of articles you may be interested in

Metamaterials and metasurfaces for designing metadevices: Perfect absorbers and microstrip patch antennas

Yahong Liu(刘亚红), Xiaopeng Zhao(赵晓鹏)
Chin. Phys. B . 2018, 27(11): 117805. **doi:** 10.1088/1674-1056/27/11/117805

High-performance lens antenna using high refractive index metamaterials

Lai-Jun Wang(王来军), Qiao-Hong Chen(陈巧红), Fa-Long Yu(余发龙), Xi Gao(高喜)
Chin. Phys. B . 2018, 27(8): 087802. **doi:** 10.1088/1674-1056/27/8/087802

Controlling flexural waves in thin plates by using transformation acoustic metamaterials

Xing Chen(陈幸), Li Cai(蔡力), Ji-Hong Wen(温激鸿)
Chin. Phys. B . 2018, 27(5): 057803. **doi:** 10.1088/1674-1056/27/5/057803

Design and theoretical study of a polarization-insensitive multiband terahertz metamaterial bandpass filter

Hai-Peng Li(李海鹏), Wen-Yue Fu(付文悦), Xiao-Peng Shen(沈晓鹏), Kui Han(韩奎), Wei-Hua Wang(王伟华)
Chin. Phys. B . 2017, 26(12): 127801. **doi:** 10.1088/1674-1056/26/12/127801

Guided mode resonance in planar metamaterials consistingof two ring resonators with different sizes

Zhen Yu(俞禛), Hang Che(陈航), Jianjun Liu(刘建军), Xufeng Jing(井绪峰), Xiangjun Li(李向军), Zhi Hong(洪治)
Chin. Phys. B . 2017, 26(7): 077804. **doi:** 10.1088/1674-1056/26/7/077804

Broadband microwave absorption properties of polyurethane foam absorber optimized by sandwiched cross-shaped metamaterial*

Long-Hui He(贺龙辉), Lian-Wen Deng(邓联文)†, Heng Luo(罗衡), Jun He(贺君), Yu-Han Li(李宇涵), Yun-Chao Xu(徐运超), and Sheng-Xiang Huang(黄生祥)

School of Physics and Electronics, Central South University, Changsha 410083, *China*

(Received 9 July 2018; revised manuscript received 3 September 2018; published online 10 November 2018)

The effect of a sandwiched cross-shaped metamaterial absorber (CMMA) on microwave absorption properties of the double-layered polyurethane foam absorber (PUFA) is investigated. Combining with the sandwiched CMMA, the bandwidth of −10-dB reflection loss for PUFA is broadened from 7.4 GHz to 9.1 GHz, which is attributed to the overlap of two absorption peaks originating from CMMA and PUFA, respectively. The values of the two absorption peaks located at 10.15 GHz and 14.7 GHz are −38.44 dB and −40.91 dB, respectively. Additionally, distribution of surface current, electromagnetic field and power loss density are introduced to investigate the absorption mechanism of the CMMA. The electromagnetic field distribution of the double-layered PUFA and the three-layered hybrid absorber are comparatively analyzed to ascertain the influence of CMMA. The results show that the proposed hybrid absorber can be applied to the anti-electromagnetic interference and stealth technology.

Keywords: polyurethane foam absorber, metamaterial, broadband microwave, absorption mechanism

PACS: 78.20.Ci, 41.20.Jb, 42.25.Ja **DOI:** 10.1088/1674-1056/27/12/127801

1. Introduction

Microwave absorbing materials adapted to broadband absorption play a vital role in many application areas, such as directive antenna,[1,2] military stealth,[3–5] and microwave circuits.[6,7] The frequency range of 8 GHz–18 GHz has received a great deal of attention thanks to its extensive application in radar system.[8–14] The polyurethane foam absorber (PUFA) has become an efficient absorber to the incident radar wave in 8 GHz–12 GHz or 12 GHz–18 GHz.[15–18] However, it is still difficult for PUFA to possess good microwave absorbing ability in the whole 8 GHz–18 GHz range. Strong electromagnetic loss and good impedance matching in a range of 8 GHz–18 GHz are still troublesome problems.

Electromagnetic metamaterials are artificially and periodically constructed sub-wavelength structures or composites. Furthermore, electromagnetic metamaterials have extraordinary electromagnetic properties, such as negative refractive index,[19,20] controlling reflection,[21,22] absorption,[23,24] and propagation[25,26] of electromagnetic waves. In 2008, Landy *et al.* put forward the metamaterial perfect absorber operating through electromagnetic resonance, and nearly 100% absorption occurred at 11.48 GHz by employing a split ring resonator on the top of the dielectric substrate supported by copper strips.[23] These sandwiched metamaterial absorbers (MMAs) also have easily adjustable electromagnetic parameters and peak absorption frequencies by changing the structural parameters of the unit cell.

Hui *et al.*[27] designed a radar absorption composite material consisting of resistive MMA and PUFA filled with short carbon fibers. The absorption bandwidth is remarkably broadened to 7 GHz for PUFAs combined with resistive MMA. However, the fabrication of the composite absorber containing resistors is relatively complicated. Some reports[28–31] have indicated that the sandwiched cross-shaped metamaterial absorber (CMMA) is polarization-insensitive and perfectly absorptive.

Motivated by these problems, we integrate CMMA and PUFAs into a triple-layered hybrid absorber in our work to realize good microwave absorption in an extended bandwidth of the whole range of 8 GHz–18 GHz. In this triple-layered hybrid absorber, the top and middle PUFAs provide good impedance matching and strong absorption in the high frequency range. The bottom metamaterial offers a resonant absorption peak combined with PUFAs, and results in wider bandwidth. The proposed design can be manipulated to support a wide variety of applications.

2. Design, fabrication, and measurement

Figure 1(a) shows a unit cell of the proposed CMMA. The designed CMMA has three functional layers: a top cross-shaped array metallic layer, a dielectric substrate, and a bottom metallic ground plane. Metal of top and bottom layer both are silver with a conductivity of 6.3×10^7 S/m. The permittivity of dielectric substrate is $4.4(1 + \mathrm{i}0.025)$. Full wave

*Project supported by the National Key Research and Development Program of China (Grant No. 2017YFA0204600), the National Natural Science Foundation of China (Grant No. 51802352), and the Fundamental Research Funds for the Central Universities of Central South University, China (Grant No. 2018zzts355).

†Corresponding author. E-mail: denglw@csu.edu.cn

© 2018 Chinese Physical Society and IOP Publishing Ltd

electromagnetic simulations were performed based on the finite element method (FEM). A floquet port was adopted at the top boundary of the unit cell to simulate a normally incident TEM plane wave. Periodic boundary conditions were used to simulate a two-dimensional periodic structure. The optimized geometric parameters marked in Figs. 1(b) and 1(c) are as follows: $P = 6.2$ mm, $l = 5.8$ mm, $w = 0.3$ mm, $t_d = 1$ mm, and $t_m = 0.035$ mm. The cross-shaped array and metallic ground plane were printed on the upper and lower surface of the dielectric substrate by the screen printing technique, respectively. Figure 2(b) shows the fabricated prototype of the CMMA.

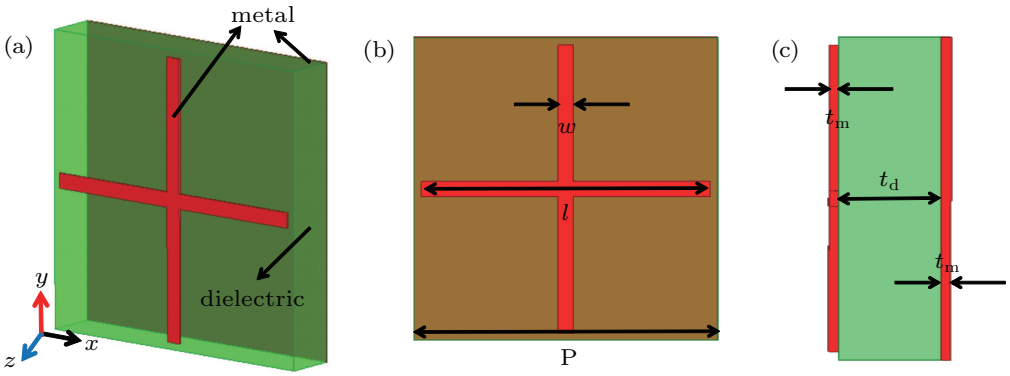


Fig. 1. (color online) Schematic description of the unit cell of the CMMA, showing (a) perspective view, (b) front view, and (c) side view.

Figure 2(a) shows the stacking order of the three-layered hybrid absorber. The proposed hybrid absorber consists of two-layered PUFAs and one-layered CMMA. The PUFA contains $PUFA_1$ filled with 3.5 wt% of polycrystalline iron fibers and $PUFA_2$ filled with 5.2 wt% of short carbon fibers. Thicknesses of the $PUFA_1$ and $PUFA_2$ are $d_1 = 2$ mm and $d_2 = 9$ mm, respectively. Thickness of the sandwiched CMMA is $d_3 = 1.07$ mm. Figure 2(b) shows the photograph of the fabricated three-layered hybrid absorber. The experimental measurements of the fabricated samples are performed by the arch measurement system in a microwave anechoic chamber. The arch measurement system is composed of an Agilent N5230A vector network analyzer and a pair of broadband antenna horns operating in the frequency band of 8 GHz–18 GHz.

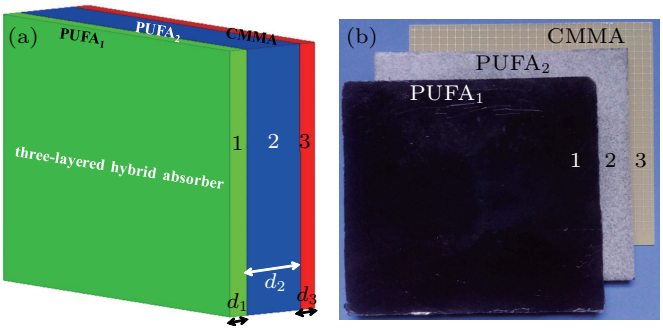


Fig. 2. (color online) (a) Stacking order and (b) photograph of three-layered hybrid absorber.

3. Results and discussion

Figure 3(a) shows the simulated and measured reflection loss curve of the proposed CMMA. The simulated reflection loss spectrum consists of a resonance peak located at 10.47 GHz with a peak reflection loss of −20.06 dB. The measured reflection loss curve presents a peak reflection loss of −17.63 dB at 10.70 GHz. This measured result is in reasonable agreement with the simulation value, except for a little blue shift of peak absorption frequency. These results indicate that the reliability of the simulated result and validity of the design of the CMMA.

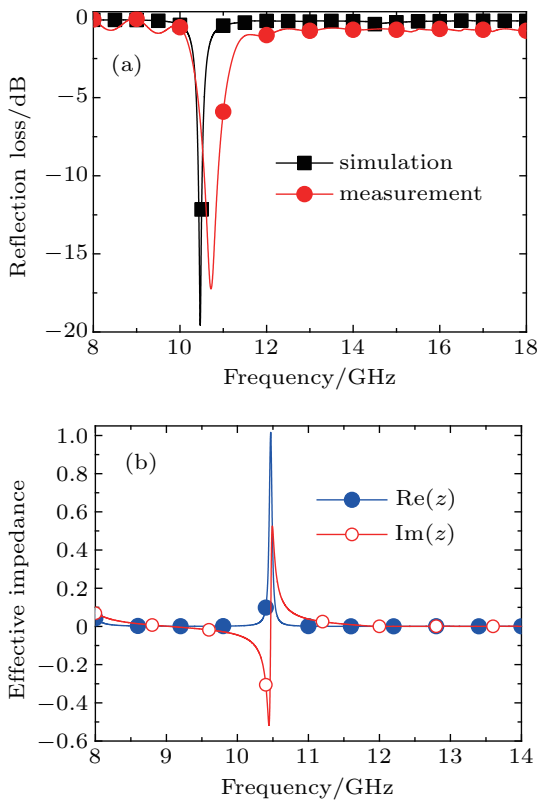


Fig. 3. (color online) (a) Simulated and measured reflection loss curve, and (b) effective input impedance of proposed CMMA.

As shown in Fig. 3(b), the effective input impedance of the proposed CMMA can be calculated from the following

formula:[32]

$$Z=\sqrt{\frac{(1+S_{11})^2-S_{21}^2}{(1-S_{11})^2-S_{21}^2}}=\frac{1+S_{11}}{1-S_{11}}\quad(\text{as}\ \ S_{21}=0),\qquad(1)$$

where S_{21} and S_{11} are the transmission coefficient and reflection coefficient, respectively. One can clearly observe that the value of the effective input impedance for the proposed CMMA at a peak frequency of 10.47 GHz is $1.07+\mathrm{j}0.07$, approaching to the required condition for ideal matching impedance $(1+\mathrm{j}0)$, where 1 indicates that the impedance of the absorber equals that of the free space and 0 means no phase difference exists between the incident electric field and magnetic field at the interface. Therefore, the proposed CMMA has good impedance matching characteristic at the peak absorption frequency of 10.47 GHz.

Figure 4 exhibits the measured reflection loss curves of samples S_1, S_2, S_3, and S_4. Here S_1 represents the $PUFA_2$, S_2 the combined sample of $PUFA_1$ and $PUFA_2$, S_3 the combined sample of $PUFA_2$ and CMMA, and S_4 the combined sample of $PUFA_1$, $PUFA_2$, and CMMA. Reflection loss of S_1 is lower than -10 dB in a frequency range from 11.75 GHz to 16.60 GHz with an effective bandwidth of 4.85 GHz. To further broaden the bandwidth of $PUFA_2$, two available methods are used. One is to load $PUFA_1$ on the top of $PUFA_2$, obtaining the sample S_2. Reflection loss lower than -10 dB for S_2 is 10.6 GHz–18 GHz with an effective bandwidth of 7.4 GHz, which is attributed to the improvement of impedance matching.[33,34] The other is to add CMMA to the bottom of $PUFA_2$, forming the sample S_3. The reflection loss curve of S_3 consists of two absorption peaks, which are located at 10.2 GHz and 12.1 GHz with peak values of -18.09 dB and -16.34 dB, respectively. Remarkably, the absorption peak located at 10.2 GHz is attributed to the CMMA. However, the effective bandwidth of -10 dB reflection loss is only 3.7 GHz for S_3. Thus, the two above-mentioned methods are combined to constitute the sample of S_4. The reflection loss lower than -10 dB for S_4 is in a frequency range from 8.9 GHz to 18 GHz with the effective bandwidth of 9.1 GHz. It is also noted that the reflection loss curve of S_4 is composed of two absorption peaks located at 10.15 GHz and 14.7 GHz with the peak values of -38.44 dB and -40.91 dB, respectively. The effective bandwidth, peak absorption frequency and corresponding reflection loss for each of the four samples are listed in Table 1 for comparison. The absorbent used in $PUFA_2$ is the short carbon fiber. The electromagnetic parameters of $PUFA_2$ depend mainly on the content of absorbent. The complex permittivity of $FUFA_2$ with 4.2, 4.7, 5.2, 5.7, and 6.2 wt% of short carbon fibers were measured and shown in Fig. 5. The values of ε' and ε'' increase with the content of absorbent increasing. The microwave absorption properties of the three-layered hybrid absorber for $PUFA_2$ filled with different mass fraction of short carbon

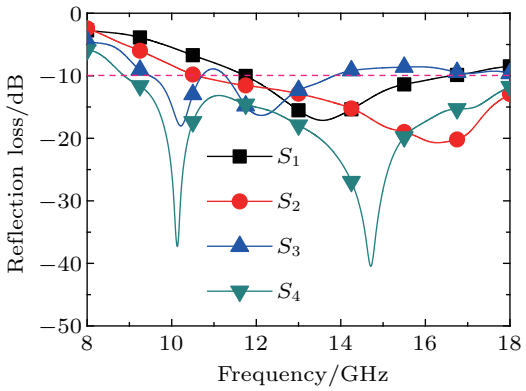


Fig. 4. (color online) Curve of measured reflection loss versus frequency of samples S_1, S_2, S_3, and S_4.

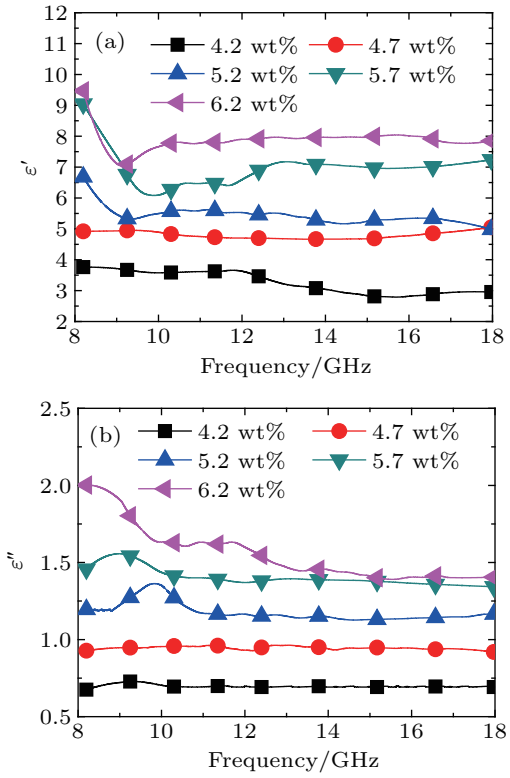


Fig. 5. (color online) (a) Real (ε') and (b) imaginary (ε'') parts of complex permittivity of $PUFA_2$ filled with different mass fractions of short carbon fiber.

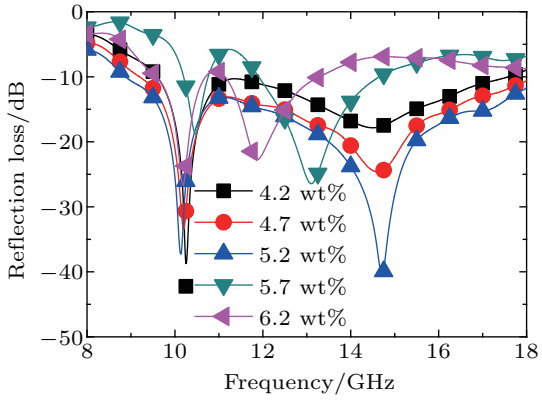


Fig. 6. (color online) Effects of $FUFA_2$ filled with different mass fractions of short carbon fiber on absorption property of three-layered hybrid absorber.

fibers are shown in Fig. 6 and listed in Table 2. It is obvious that the −40.91 dB of peak reflection loss and 9.1 GHz of optimal effective bandwidth appear at 5.2 wt% of short carbon fiber. Thus, moderate dielectric properties of $PUFA_2$ are beneficial to good absorption ability. A comparison between microwave absorption performance of previous work and that of our work is given in Table 3.

Table 1. Microwave absorption performance of samples S_1, S_2, S_3, and S_4.

Samples	Effective bandwidth/GHz	Peak absorption frequency/GHz	Corresponding reflection loss/dB
S_1	4.85	13.55	–17.13
S_2	7.40	16.30	–20.68
S_3	3.70	10.20, 12.10	–18.09, –16.34
S_4	9.10	10.15, 14.70	–38.44, –40.91

Table 2. Microwave absorption properties of three-layered hybrid absorber of $PUFA_2$ filled with different mass fractions of short carbon fiber.

Absorbent	Mass fraction/wt%	Effective bandwidth/GHz	Peak absorption frequency/GHz	Corresponding reflection loss/dB
Carbon fiber	4.2	7.95	10.25, 14.50	–42.22, –17.84
Carbon fiber	4.7	8.80	10.20, 14.60	–34.73, –24.65
Carbon fiber	5.2	9.10	10.15, 14.70	–38.44, –40.91
Carbon fiber	5.7	4.25	10.45, 13.10	–18.96, –26.50
Carbon fiber	6.2	3.65	10.20, 11.85	–27.16, –22.74

Table 3. Comparison between microwave absorption performances of previous work and our work.

Effective bandwidth/GHz	Peak absorption frequency/GHz	Corresponding reflection loss/dB	Reference
7.0	8.70, 11.5	–24, –23	[27]
9.1	10.15, 14.70	–38.44, –40.91	This work

According to our analyses of the four samples, the bandwidth expansion of the double-layered PUFAs is attributed to the fact that the absorption peak of the CMMA is superimposed on the absorption peak of the PUFAs. To comprehend the absorption mechanism of the CMMA, the surface current distribution of the top and bottom metallic layers at 10.47 GHz are presented in Figs. 7(a) and 7(b), respectively. Figure 7(a) shows that the induced surface current flows in down-up direction on the top surface of the CMMA, activated by the external electromagnetic field. The flow direction of the top surface current indicates that the induced charges concentrate on the upper and lower edges of the cross-shaped structure. Conversely, the opposite charges are correspondingly formed on the bottom surface of the CMMA, and the induced surface current flows in up-down direction on the bottom surface of the CMMA, as shown in Fig. 7(b). Evidently, the induced surface current on the top and bottom metallic layer constitute the circulating current loops. Consequently, these current loops across the sandwiched CMMA lead to strong magnetic coupling resonance.[28–30,32] Additionally, the distribution of the magnetic field and the surface power loss density of the top and bottom metallic layers at 10.47 GHz are shown in Figs. 7(c)–7(f). As shown in Figs. 7(c) and 7(d), the magnetic field of both the top and bottom metallic layer are distributed along the direction of induced surface current. It is observed in Figs. 7(e) and 7(f) that the surface loss density distribution basically coincides with the magnetic field distribution. Therefore, the top and bottom metallic layers are responsible for the attenuation of the magnetic field energy at 10.47 GHz. The specific loss mechanism is ohmic loss for the finite conductivity of the top and bottom metals.

Figures 8(a) and 8(b) show the electric field distribution of the top and bottom metallic layer at 10.47 GHz, respectively. Owing to the accumulation of a large number of electric charges along the direction of induced surface current, the electric field intensity is stronger on the upper and lower edges of the cross-shaped structure and the bottom metallic layer, which forms the effective parallel plate capacitors with the capacitance C_m. The capacitance $C_m = \varepsilon w l'/t_s$, where $l' = c_1 l$ with the numerical factor c_1 ranging from 0.2 to 0.3, l being the cross length, w is the cross width, and t_s is the dielectric layer thickness. Additionally, the gap capacitance C_e is generated between the neighboring cross-shaped structures. The capacitance $C_e = \pi\varepsilon w/\ln(b/t_m)$, where t_m is the thickness of each metallic layer and b is the space of the neighboring crosses. The inductance L of the top and bottom metallic layer are related to the surface current. The specific calculation formula of inductance is $L = \mu(t_s/w)l$. Therefore, an equivalent circuit model for the unit cell of cross-shaped array is established as shown in Fig. 8(c) (in which the resistance elements are omitted for simplicity). To further understand the role of the middle dielectric substrate in the CMMA's absorption performance, the distribution of the magnetic field, electric field, and volume power loss density of the middle dielectric substrate are examined in Figs. 8(d)–8(f). The magnetic field distribution shown in Fig. 8(d) is similar to these of the top and bottom metallic layer. The induced electric field has high magnitude in the areas between neighboring unit cells along the y-direction [see Fig. 8(e)]. Therefore, the incident electromagnetic wave is obviously dissipated inside the spacer of the dielectric substrate around specific areas, where the induced charges are densely accumulated in the formed effective

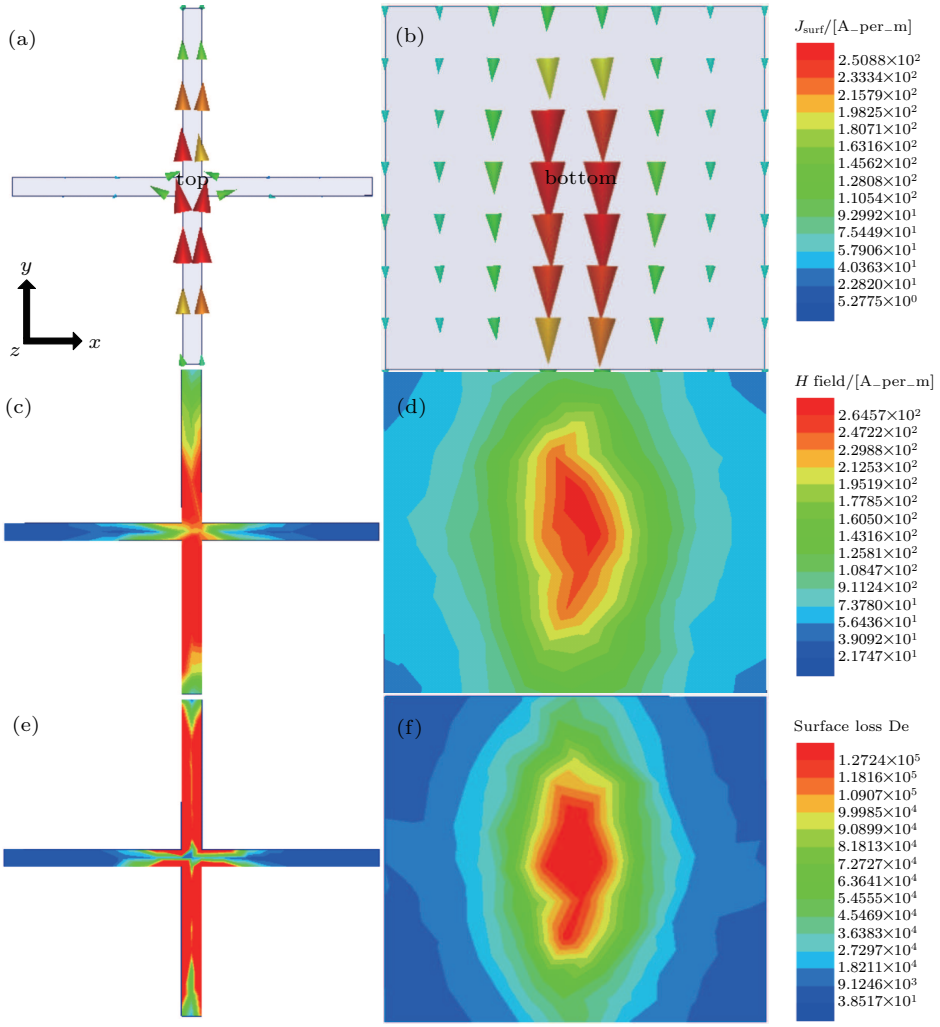


Fig. 7. (color online) (a) and (b) Surface current distribution, (c) and (d) magnetic field distribution, and (e) and (f) surface power loss density distribution of the top and bottom metallic layer for CMMA at 10.47 GHz.

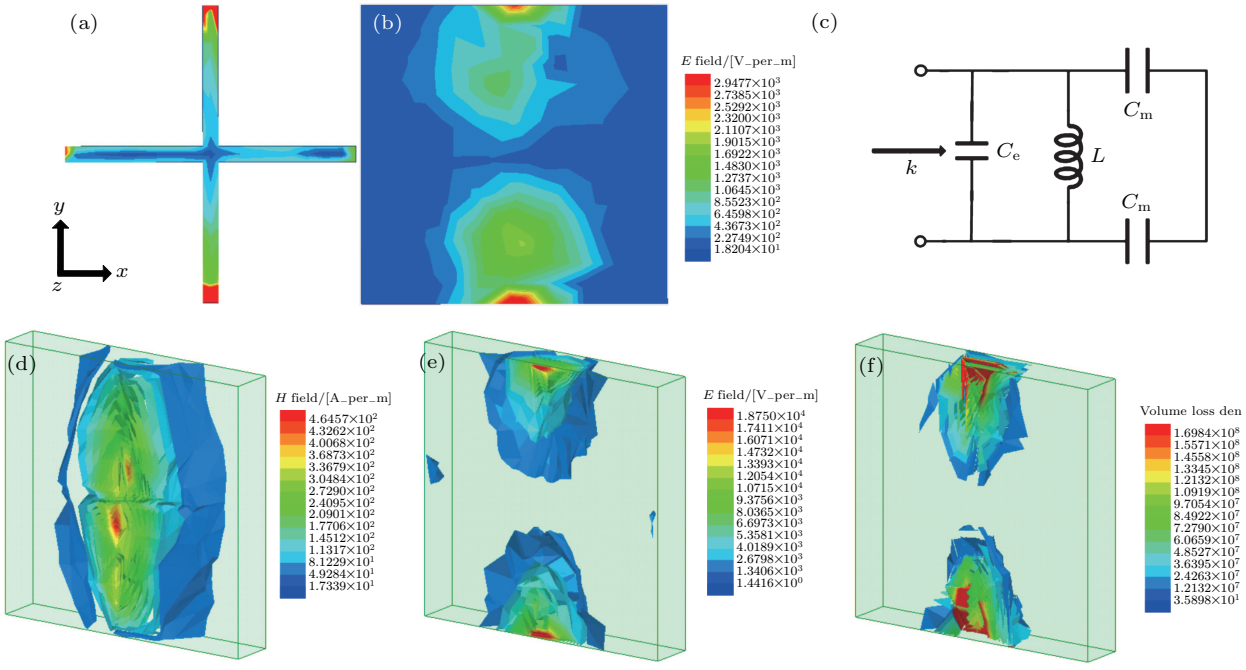


Fig. 8. (color online) (a) and (b) Electric field distribution of top and bottom metallic layer at 10.47 GHz, (c) equivalent circuit model of the unit cell of proposed CMMA, (d) magnetic field distribution, (e) electric field distribution, and (f) volume power loss density distribution of middle dielectric substrate of the CMMA at 10.47 GHz.

parallel plate capacitors [see Fig. 8(c)]. It is also observed that the volume power loss density distribution [see Fig. 8(f)] coincides roughly with the electric field distribution [see Fig. 8(e)]. Therefore, the dielectric substrate of the CMMA is responsible for the attenuation of the electric field at 10.47 GHz. In addition, previously reported work[35] has indicated that the dielectric loss plays a dominate role in electromagnetic energy attenuation for the CMMA.

The electromagnetic field distribution of the double-layered PUFAs and the three-layered hybrid absorber have been presented at 10.47 GHz, as shown in Figs. 9(a) and 9(b), respectively. It is obvious that the electric field of the double-layered PUFAs is distributed uniformly in the x–y plane, while the electric field of the three-layered hybrid absorber concentrates around the CMMA. The magnetic field distributes similar to the electric field distributions are shown in Figs. 9(c) and 9(d) respectively. Thus, CMMA is beneficial to aggregating the electromagnetic field, resulting from the resonance effect of CMMA.[8,36–38]

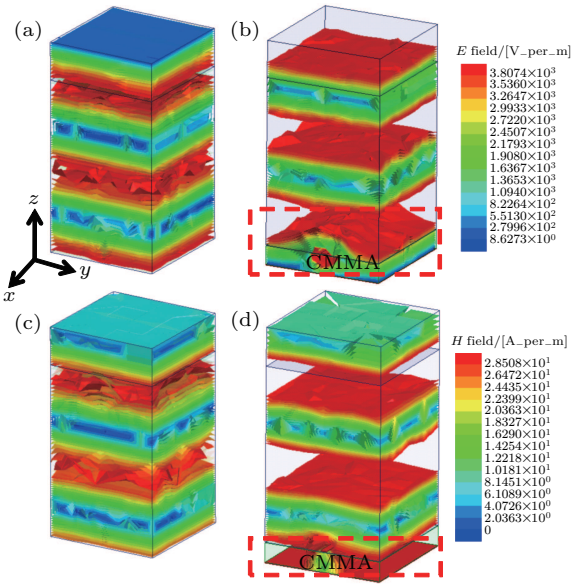


Fig. 9. (color online) Electric field distribution of (a) double-layered PUFAs and (b) three-layered hybrid absorber at 10.47 GHz. Magnetic field distribution of (c) double-layered PUFAs and (d) three-layered hybrid absorber at 10.47 GHz.

4. Conclusions

The three-layered hybrid absorber provides a broad absorption bandwidth of 9.1 GHz in a range from 8.9 GHz to 18 GHz with a reflection loss of lower than −10 dB. The reflection loss of the three-layered hybrid absorber has two minimum values of −38.44 dB and −40.91 dB located at 10.15 GHz and 14.70 GHz, respectively. The experimental measurements demonstrate that the microwave absorption bandwidth is effectively broadened for PUFA combined with CMMA. The absorption mechanism of the CMMA is ohmic loss from the top or bottom metallic layer and the dielectric loss from the middle dielectric substrate. These results pave an alternative effective way to the broadband stealth and anti-electromagnetic interference technology.

References

[1] Li Y Q, Zhang H, Fu Y Q and Yuan N C 2008 *IEEE Anten. Wirel. Propag. Lett.* **7** 473
[2] Wang F, Jiang W, Hong T, Xue H, Gong S and Zhang Y 2014 *IET Microw. Anten. Propag.* **8** 491
[3] Wu K H, Cheng K F, Wang J C and Chang Y C 2017 *Mater. Express* **7** 500
[4] He J, Deng L W, Liu S, Yan S Q, Luo H, Li Y H, He L H and Huang S X 2017 *J. Magn. Magn. Mater.* **444** 49
[5] Deng L W, Ding L, Zhou K S, Huang S X, Hu Z W and Yang B C 2011 *J. Magn. Magn. Mater.* **323** 1895
[6] Perez D, Gil I, Gago J, Fernandez-Garcia R, Balcells J, Gonzalez D, Berbel N and Mon J 2012 *IEEE Trans. Compon. Pack. Manuf. Technol.* **2** 240
[7] Nesimoglu T and Sabah C 2017 *IEEE Trans. Circuits Syst. II-Express Briefs* **63** 89
[8] Cheng Y Z, Gong R Z, Nie Y and Wang X 2012 *Chin. Phys. B* **21** 127801
[9] Wen B, Zhao J J, Duan Y P, Zhang X G, Zhao Y B, Dong C, Liu S H and Li T J 2006 *J. Phys. D: Appl. Phys.* **39** 1960
[10] Liu X G, Or S W, Ho S L, Cheung C C, Leung C M, Han Z, Geng D Y and Zhang Z D 2012 *J. Alloys Compd.* **531** 9071
[11] Ohlan A, Singh K, Chandra A and Dhawan S K 2008 *Appl. Phys. Lett.* **93** 205
[12] Zhu Z T, Sun X, Li G X, Xue H R, Guo H, Fan X L, Pan X C and He J P 2015 *J. Magn. Magn. Mater.* **377** 95
[13] Singh P, Babbar V K, Razdan A, Puri R K and Goel T C 2000 *J. Appl. Phys.* **87** 4362
[14] Sudeep P M, Vinayasree S, Mohanan P, Narayanan T N and Anantharaman M R 2015 *Appl. Phys. Lett.* **106** 061301
[15] Abbas S M, Dixit A K, Chatterjee R and Goel T C 2007 *J. Magn. Magn. Mater.* **309** 20
[16] Cao C M, Dong C H, Yao J L and Jiang C J 2018 *Chin. Phys. B* **27** 017503
[17] Zhao B, Han Q and Zhu Y 2013 *Express Polym. Lett.* **7** 212
[18] Gupta K K, Abbas S M, Goswami T H and Abhyankar A C 2014 *J. Magn. Magn. Mater.* **362** 216
[19] Smith D R, Pendry J B and Wiltshire M C 2004 *Science* **305** 788
[20] Valentine J, Zhang S, Zentgraf T, Ulin-Avila E, A Genov D, Bartal G and Zhang X 2008 *Nature* **455** 376
[21] Hao J M, Yan W and Qiu M 2010 *Appl. Phys. Lett.* **96** 4184
[22] Chen H T, Zhou J F, O'Hara J F, Chen F, Azad A K and Taylor A J 2010 *Phys. Rev. Lett.* **105** 073901
[23] Landy N I, Sajuyigbe S, Mock J J, Smith D R and Padilla W J 2008 *Phys. Rev. Lett.* **100** 207402
[24] Gu S, Barrett J P, H, T H, Popa B I and Cummer S A 2010 *J. Appl. Phys.* **108** 064913
[25] Ozbay E, Aydin K, Cubukcu E and Bayindir M 2003 *IEEE Trans. Anten. Propag.* **51** 2592
[26] Agranovich V M, Shen Y R, Baughman R H and Zakhidov A A 2004 *Phys. Rev. B* **69** 1124
[27] Hui Y C, Wang C Q and Huang X Z 2015 *Acta Phys. Sin.* **64** 218102 (in Chinese)
[28] Cheng Y Z, Yang H L, Cheng Z Z and Wu N 2011 *Appl. Phys. A: Mater. Sci. Process.* **102** 99
[29] Cheng Y Z, Yang H L, Cheng Z Z and Xiao B X 2011 *Photon. Nanostruct.* **9** 8
[30] Ma W, Wen Y and Yu X 2013 *Opt. Express* **21** 30724
[31] Li Z, Stan L, Czaplewski D A, Yang X and Gao J 2018 *Opt. Express* **26** 5616
[32] Smith D R, Vier D C, Koschny T and Soukoulis C M 2005 *Phys. Rev. E* **71** 036617
[33] Wu J S, Duan Y P and Xi Q 2017 *J. Mater. Sci.: Mater. Electron.* **28** 3075
[34] Ma J N, Zhang X M, Liu W and Ji G B 2016 *J. Mater. Chem. C* **4** 11419
[35] Liu X L, Starr T, Starr A F and Padilla W J 2010 *Phys. Rev. Lett.* **104** 207403
[36] Bu D D, Yue C S, Zhang G Q, Hu Y T and Dong S 2016 *Chin. Phys. B* **25** 067802
[37] Xu Y S, Bie S W, Jiang J J, Xu H B, Wang D and Zhou J 2014 *Acta Phys. Sin.* **63** 205202 (in Chinese)
[38] Zhang K L, Hou Z L, Bi S and Fang H M 2017 *Chin. Phys. B* **26** 127802